catalysts

MDPI

Article

Natural Pyrolusite-Catalyzed Ozonation for Nanoplastics Degradation

Victor Mello [1,2,*], Julia Nieto-Sandoval [2], Márcia Dezotti [1] and Carmen Sans [2,*]

[1] Chemical Engineering Program/COPPE, Federal University of Rio de Janeiro, Av. Horácio Macedo 2030, Bloco G, Cidade Universitária, Rio de Janeiro 21941-914, Brazil; mdezotti@peq.coppe.ufrj.br
[2] Department of Chemical Engineering and Analytical Chemistry, Faculty of Chemistry, Universitat de Barcelona, C/Martí i Franqués 1, 08028 Barcelona, Spain; julia.nietosandoval@ub.edu
* Correspondence: victormello@peq.coppe.ufrj.br (V.M.); carmesans@ub.edu (C.S.); Tel.: +55-219-7362-3876 (V.M.)

Abstract: The increasing prevalence of polystyrene nanoplastics (PSNPs) in aquatic environments poses significant risks due to their persistence and potential toxicity. Conventional water treatment methods have proven ineffective in removing these emerging pollutants, highlighting the urgent need for sustainable and efficient treatment. This study investigates the application of catalytic ozonation using natural pyrolusite (n-MnO_2) and oxalic acid (OA) as a co-catalyst for the environmentally friendly degradation of PSNPs. Key operational parameters, including pH, applied ozone dose, pyrolusite dosage, and OA concentration, were systematically evaluated. Results demonstrate that the MnO_2 + OA + O_3 system enhances the generation of reactive oxygen species (ROS), leading to improved PSNP removal while maintaining the applied ozone dose compared to the single ozonation reaction. The highest TOC removal of 75% was achieved within 30 min of treatment under optimal conditions (pH = 4, [MnO_2] = 0.5 g L^{-1}, [OA] = 10 mg L^{-1}, and ozone dose of 37.5 mg min^{-1}), with significant turbidity reduction, indicating both chemical and physical degradation of PSNPs. Catalyst reusability after three consecutive cycles confirmed minimal loss in activity, reinforcing its potential as a sustainable catalytic system. These findings highlight natural MnO_2-driven catalytic ozonation as a green and effective strategy for nanoplastic removal in water treatment applications.

Keywords: catalytic ozonation; polystyrene nanoplastics; natural manganese dioxide; water treatment; advanced oxidation processes; green catalysis

Academic Editors: Hugo Olvera Vargas, José Ignacio Lombraña and Sandra Yazmin Arzate Salgado

Received: 28 March 2025
Revised: 13 May 2025
Accepted: 16 May 2025
Published: 21 May 2025

Citation: Mello, V.; Nieto-Sandoval, J.; Dezotti, M.; Sans, C. Natural Pyrolusite-Catalyzed Ozonation for Nanoplastics Degradation. *Catalysts* **2025**, *15*, 502. https://doi.org/10.3390/catal15050502

1. Introduction

The widespread production and use of plastic materials have led to the increasing presence of microplastics (MPs) and nanoplastics (NPs) in aquatic environments. NPs, typically defined as plastic particles smaller than 1 µm, are particularly concerning due to their high surface-area-to-volume ratio, enhanced chemical reactivity, and ability to cross biological barriers, thereby posing significant environmental and health risks [1]. Unlike MPs, which are often removed to a large extent by conventional water treatment processes, NPs are more difficult to remove and have been detected in drinking water, freshwater bodies, and marine ecosystems [2]. Due to their small size, NPs can penetrate cellular membranes, cause oxidative stress, and disrupt metabolic processes in aquatic organisms [3]. Recognizing these risks, regulatory bodies like the European Union (EU) have implemented guidelines to limit and monitor plastic particles in water systems.

For instance, the EU Drinking Water Directive (Directive (EU) 2020/2184) mandates the monitoring of MPs in drinking water, and similar measures are being explored for NPs [4].

Among the various types of NPs, polystyrene nanoplastics (PSNPs) have garnered significant attention due to their extensive use in packaging, insulation, and disposable consumer products. Polystyrene (PS) is known for its chemical stability, hydrophobicity, and resistance to biodegradation, making PSNPs particularly persistent in aquatic environments [5]. Once released into aquatic systems, PSNPs undergo weathering and fragmentation, further increasing their abundance and bioavailability in water sources [6]. Their persistence and toxicity underscore the urgent need for efficient removal strategies. Conventional water treatment processes, such as filtration, coagulation, and sedimentation, are not sufficient to eliminate NPs completely due to their small size and colloidal nature [7]. As a result, advanced oxidation processes (AOPs) have emerged as promising alternatives for NPs removal.

Ozonation is one of the most widely studied AOPs, as ozone (O_3) is a strong oxidizing agent capable of decomposing a broad range of organic pollutants in water. However, the direct ozonation of PSNPs is limited due to the selective reactivity of molecular O_3. Ozone preferentially reacts with electron-rich sites, such as double bonds or amine groups, but it is less effective at breaking down stable aromatic structures like the benzene rings found in PS [8]. This limitation highlights the need for an approach that generates more reactive species capable of non-selective oxidation.

To overcome the limitations of direct ozonation, catalytic ozonation has been proposed as an enhanced AOP. Catalytic ozonation accelerates the decomposition of O_3 into reactive oxygen species (ROS) such as hydroxyl radicals ($^{\bullet}OH$) and superoxide radicals ($O_2^{\bullet-}$), which exhibit higher oxidation potential and non-selective reactivity [9,10]. These ROS are capable of breaking stable chemical bonds, including aromatic structures, thereby facilitating the degradation of PSNPs. Catalysts such as transition metal oxides have been widely investigated due to their ability to activate O_3. Among these, manganese dioxide (MnO_2) has gained attention for its low cost, availability, and environmental compatibility [11,12]. However, studies on the catalytic ozonation of NPs remain limited. To the best of our knowledge, only the work by Li et al. (2023) has addressed this issue in the literature by heterogenous catalytic ozonation, showing promising results on PSNPs molecular weight decreasing by ozonation in the presence of a CeOx@MnOx catalyst [13]. Nevertheless, no data about further mineralization were reported.

Natural pyrolusite, a naturally occurring mineral form of MnO_2, is particularly attractive as it provides a cost-effective and abundant source of MnO_2, thereby supporting the scalability of catalytic ozonation for water treatment [14,15]. The efficiency of catalytic ozonation can be further enhanced by introducing oxalic acid (OA) as a co-catalyst. OA forms stable Mn^{3+}–oxalate complexes that prevent the deactivation of the catalyst and maintain the continuous production of ROS. OA also acts as an additional radical promoter, promoting the formation of highly reactive $^{\bullet}OH$ and other oxygen species. This synergy between MnO_2, OA, and O_3 has improved the degradation of organic micropollutants in previous studies [16,17]. The mechanism underlying this enhancement is linked to the regeneration of redox sites on MnO_2, as the Mn^{3+}–oxalate complex facilitates the cycling of Mn from Mn^{3+} to Mn^{4+}, thereby sustaining catalytic activity.

Thus, this study aims to investigate the efficiency of heterogeneous catalytic ozonation for PSNPs removal using n-MnO_2 as a catalyst. In order to enhance PSNPs degradation, OA was incorporated into the system as a co-catalyst. A complete operating conditions study has been carried out to evaluate the effect of pH, catalyst dose, O_3 dose, and the presence and concentration of OA on PSNPs removal. The study also assesses catalyst reusability

over consecutive cycles, offering insights into the long-term stability and practicality of catalytic ozonation for NPs removal in water treatment processes.

2. Results and Discussion

2.1. Pyrolusite Characterization

The characterization of n-MnO_2 was conducted using three analytical techniques: point of zero charge (pH_{PZC}), Fourier-transform infrared spectroscopy (FTIR), and X-ray photoelectron spectroscopy (XPS). Figure 1 shows the results obtained for each technique.

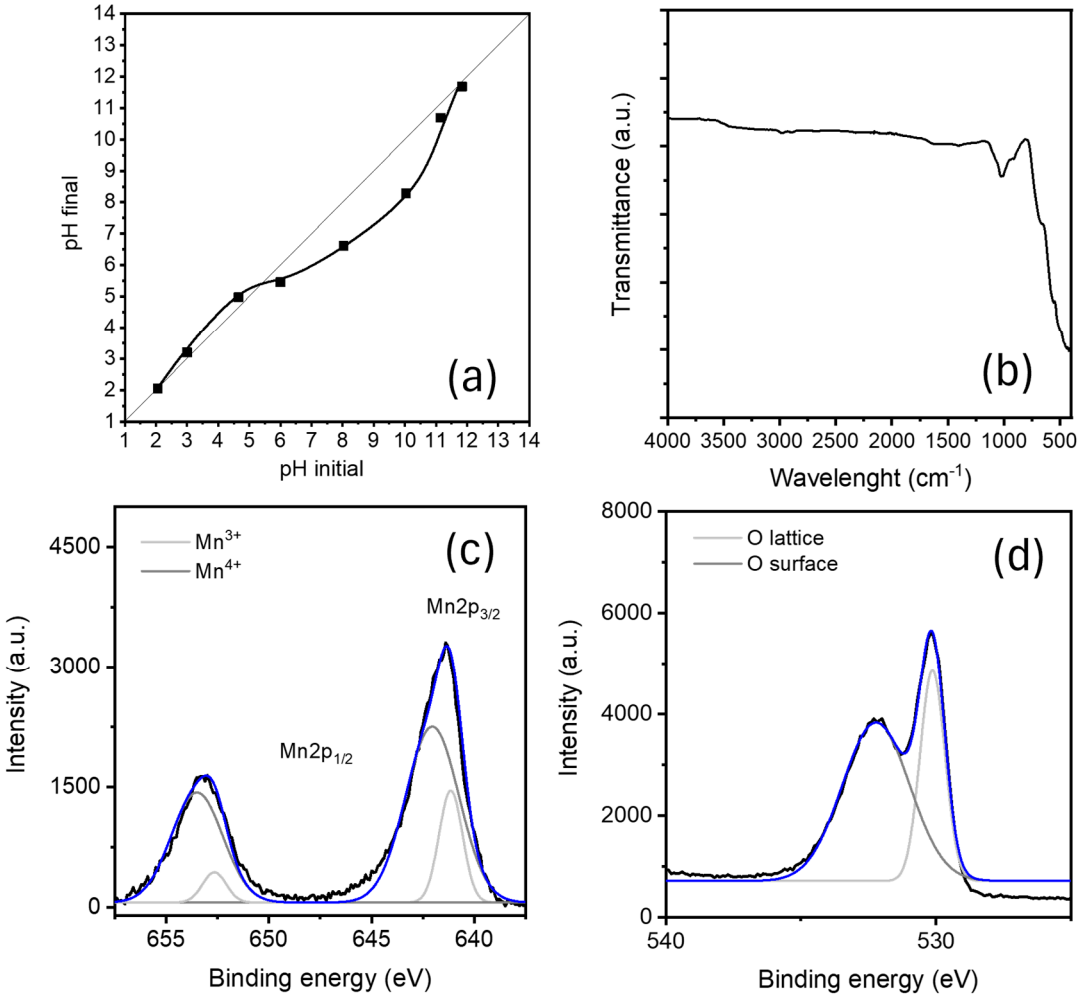

Figure 1. Pyrolusite characterization: pH_{PZC} (**a**), FTIR spectrum (**b**), Mn2p XPS spectra (**c**), and O1s XPS spectra of n-MnO_2 (**d**). In (**a**), black squares represent experimental pH values and the solid line corresponds to the linear fit used to determine the point of zero charge. In (**c**) and (**d**), the blue line is the experimental XPS spectrum, while the gray curves represent the deconvoluted component peaks.

The pH_{PZC} of pyrolusite was determined to be 5.5 (Figure 1a), indicating that below this pH, the surface of MnO_2 is positively charged, while above it, the surface becomes negatively charged. This charge variation significantly affects the adsorption of ionic species and, consequently, the formation of surface complexes. At pH values below the pH_{PZC}, the positively charged MnO_2 surface enhances the adsorption of negatively charged species, such as oxalate ions derived from the dissociation of OA. This electrostatic attraction facilitates the formation of surface complexes between MnO_2 and oxalate ions, which is crucial for catalytic processes [18,19]. The study by Omorogie et al. (2022) has demonstrated that the adsorption of anionic dyes onto MnO_2-modified biomass is more effective at pH

levels below the pH_{PZC}, attributed to the increased positive surface charge promoting anion adsorption [20]. Conversely, at pH values above the pH_{PZC}, the MnO_2 surface acquires a negative charge, which can lead to repulsion of anionic species like oxalate ions, thereby reducing the efficiency of complex formation.

The FTIR spectrum (Figure 1b) reveals two characteristic peaks confirming MnO_2 presence in the pyrolusite sample. The peak at 1100 cm^{-1} is attributed to the coordination of manganese by hydroxyl groups (O-H), which are known to participate in surface-mediated catalytic reactions [21,22]. The second prominent peak, observed at approximately 500 cm^{-1}, corresponds to the stretching vibrations of Mn–O and Mn–O–Mn bonds, indicating the presence of octahedral MnO_6 structures characteristic of MnO_2 [23,24]. Similar FTIR signatures have been reported in other studies involving natural and synthetic manganese oxides used as ozonation catalysts [19,25].

The XPS analysis of the Mn2p region of n-MnO_2 (Figure 1c) revealed two primary peaks corresponding to $Mn2p_{3/2}$ and $Mn2p_{1/2}$, with a binding energy difference (ΔE) of 11.5 eV. This energy separation is characteristic of MnO_2 in the Mn^{4+} oxidation state [26,27]. The deconvolution of the $Mn2p_{3/2}$ peak showed contributions from two distinct components, indicating the presence of both Mn^{3+} and Mn^{4+} species. The calculated Mn^{3+}/Mn^{4+} ratio was 0.8, confirming that Mn^{4+} is the predominant oxidation state in the n-MnO_2 sample. The prevalence of Mn^{4+} is consistent with the mineralogical composition of pyrolusite and its catalytic activity in O_3 decomposition [28,29]. Mn^{4+} sites on the surface of pyrolusite facilitate the activation of ozone molecules, generating ROS such as •OH and $O_2•^-$, which contribute to the degradation of organic pollutants [30,31]. Moreover, the presence of Mn^{3+} indicates a redox-active surface, capable of cycling between Mn^{4+} and Mn^{3+} states during catalytic ozonation. This redox behavior enhances O_3 decomposition and maintains the catalytic activity of pyrolusite over multiple reaction cycles [19,31]. The presence of both oxidation states is essential for sustaining ROS generation and achieving efficient organic pollutants degradation. The O1s XPS spectrum of the n-MnO_2 catalyst, presented in Figure 1d, provides critical insights into the surface oxygen species involved in the catalytic ozonation process. The deconvolution of the spectrum reveals the presence of distinct peaks corresponding to different oxygen environments, which directly influence the catalyst's reactivity and its ability to generate ROS during ozonation. The O1s spectrum exhibits two primary peaks, which can be attributed to distinct oxygen species associated with the MnO_2 surface. The first peak (~529.5 eV, lower binding energy) corresponds to lattice oxygen (O_2^-) bound within the MnO_2 crystal structure [32]. Lattice oxygen is characteristic of metal oxides and is essential for the redox cycling of manganese species (Mn^{3+}/Mn^{4+}) that facilitates O_3 decomposition and ROS generation [32,33]. The dominance of this peak confirms the crystalline nature of the MnO_2 phase in pyrolusite, which serves as the active site for catalytic reactions. The second main peak (~531.5 eV, higher binding energy) is attributed to surface-adsorbed oxygen species, including hydroxyl groups (–OH) and chemisorbed oxygen (O^-) [34,35]. These species play a critical role in O_3 activation by providing sites for ozone adsorption and subsequent radical formation. Hydroxyl groups, in particular, act as proton donors and facilitate the formation of •OH, which are highly reactive toward organic pollutants like PSNPs [32,36]. The distribution of oxygen species observed in the O1s spectrum aligns with the previously determined point of zero charge (pH_{PZC} = 5.5). In acidic pH conditions (e.g., pH 4), the surface hydroxyl groups (O–H) are more likely to be protonated, promoting the adsorption of negatively charged ozone species (O_3^-) and oxalate ions (OA) [37]. The presence of chemisorbed oxygen species at ~531.5 eV supports this hypothesis, indicating a surface environment conducive to ROS production and organic pollutants degradation.

The surface oxygen groups detected via XPS are consistent with the FTIR results, which revealed a characteristic peak at 1100 cm^{-1}, associated with hydroxyl group coordination. This corroborates the presence of reactive –OH groups on the pyrolusite surface, essential for catalytic ozonation mechanisms [25].

2.2. Catalytic Ozonation of Polystyrene Nanoplastics

Previous studies have demonstrated that single ozonation effectively reduces the molecular weight of PSNPs, as evidenced mainly by gel permeation chromatography (GPC) analyses [38,39]. For instance, Li et al. (2022) observed a 99.9% reduction in molecular weight and a 42.7% mineralization of nano-sized PS after 240 min of ozonation under typical disinfection conditions [38]. Similarly, research by Li et al. (2023) reported that ozonation achieved a 32% decrease in PSNP molecular weight within the first 10 min, which increased to 51.67% in the presence of a MnOx catalyst, and further to 73.33% when employing a CeOx@MnOx catalyst [13]. However, complete removal of PSNPs is not guaranteed by ozonation alone. In fact, as demonstrated by Nieto-Sandoval (2024), single ozonation can lead to the formation of smaller NP particles, potentially increasing their environmental persistence and toxicity [39]. Therefore, to comprehensively assess NP removal, this study focuses on total organic carbon (TOC) reduction, providing deeper insights into the mineralization and effective elimination of PSNPs by heterogeneous catalytic ozonation.

In this study, the removal of PSNPs was evaluated under different systems, including single ozonation (O_3), catalytic ozonation (MnO_2 + O_3), ozonation with oxalic acid (OA + O_3), and catalytic ozonation with oxalic acid (MnO_2 + OA + O_3). Additionally, the individual effects of the catalysts, MnO_2 and OA, are presented to isolate their individual contributions to the removal process. Figure 2a shows TOC, and Figure 2b shows turbidity removal efficiencies for PSNPs under these systems. The initial TOC of the reactions containing 20 mg L^{-1} of PSNPs was 16.2 ± 1.7 mg L^{-1}, and the initial turbidity was 80.7 ± 3 NTU. The comparison provides insight into the relative feasibility of each treatment, highlighting the synergistic effects achieved when MnO_2 and OA are combined during catalytic ozonation. The subsequent analysis focuses on the key differences in TOC and turbidity removal efficiencies observed across these treatments, as well as the mechanistic implications of the results.

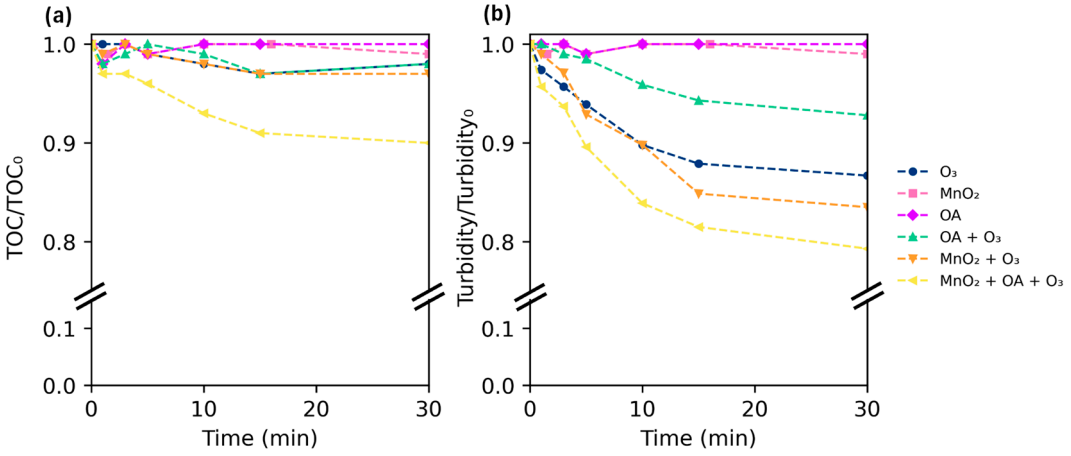

Figure 2. TOC (**a**) and turbidity (**b**) evolution upon PSNPs removal under different systems: O_3, MnO_2, OA, OA + O_3, MnO_2 + O_3, and MnO_2 + OA + O_3 ($[PSNPs]_0$ = 20 mg L^{-1}; O_3 dose= 7.5 mg min^{-1}; $[MnO_2]_0$ = 0.25 g L^{-1}, $[OA]_0$ = 2.5 mg L^{-1}; T = 20 °C; pH = 7).

Single ozonation showed limited efficacy, with TOC/TOC_0 decreasing by only 2% within 30 min, confirming ozone's inability to mineralize PSNPs alone. A similar trend was observed for turbidity, which decreased from 1.00 to 0.87, suggesting minor physical disaggregation of PSNP aggregates. This limited performance is attributed to the selective nature of molecular O_3, which reacts with electron-rich moieties but struggles to break down the stable aromatic structure of PS [8]. Similar findings were reported by Li et al. (2022), who demonstrated that significant PSNP degradation by ozonation requires extended contact times (up to 240 min) to achieve molecular weight reductions [38].

The individual application of MnO_2 and OA also resulted in negligible TOC and turbidity reduction (TOC/TOC_0 = 0.99 and 1.00; $turbidity/turbidity_0$ = 0.99 and 1.00, respectively). In the absence of O_3, MnO_2 lacks an oxidizing mechanism, and OA alone does not promote PSNP oxidation. Even the OA + O_3 combination yielded no improvement (TOC/TOC_0 = 0.99; $turbidity/turbidity_0$ = 0.90), indicating that OA alone is not sufficient to enhance ozone-based degradation.

A slight improvement was observed with the MnO_2 + O_3 system, reducing TOC/TOC_0 to 0.97 and turbidity to 0.84. MnO_2 serves as a heterogeneous catalyst that decomposes O_3 into reactive oxygen species (ROS) [18,40], including $^{\bullet}OH$ and $O_2^{\bullet-}$, which exhibit higher oxidation potential and broader reactivity than ozone alone. The redox cycling between Mn^{3+} and Mn^{4+} on the catalyst surface supports the generation of these ROS, as shown in Equation (1):

$$MnO_2 + O_3 \rightarrow MnO_2{}^* + O_2 + ROS \quad (1)$$

where $MnO_2{}^*$ refers to Mn^{3+} on the catalyst surface. The reactivity of these radicals toward PSNPs leads to oxidative cleavage of polymeric chains, promoting fragmentation and partial mineralization.

The most significant enhancement occurred in the MnO_2 + OA + O_3 system, which achieved a TOC/TOC_0 reduction of 0.90 and $turbidity/turbidity_0$ = 0.81 after 30 min. Notably, the system did not reach a constant value, indicating that TOC/TOC_0 continued to decrease throughout the reaction time. This system benefits from the synergistic interaction between MnO_2 and OA. Oxalic acid contributes by forming Mn^{3+}–oxalate complexes (Equation (2)) that maintain the redox cycling and prevent catalyst deactivation [19]:

$$Mn^{3+} + C_2O_4{}^{2-} \rightarrow Mn^{3+}(oxalate)_{complex}. \quad (2)$$

Additionally, OA acts as a radical promoter under acidic conditions, facilitating further ROS formation. Studies by Andreozzi et al. (1998) and Xiao et al. (2008) have shown that low-molecular-weight organic acids like OA enhance ozone decomposition by donating electrons and stabilizing redox intermediates [9,41]. This synergy promotes the sustained generation of ROS, leading to both polymer chain cleavage and partial mineralization of PSNPs.

In line with these findings, the formation of ROS is strongly supported by the catalytic conditions employed and the previous literature involving Mn-based systems. Under acidic pH, MnO_2 facilitates the decomposition of O_3 into •OH and $O_2\bullet^-$ via redox cycling between Mn^{4+} and Mn^{3+}, particularly when oxalate ions are present to stabilize Mn^{3+} intermediates. Prior studies have shown that OA promotes additional ROS formation by accelerating ozone decomposition and enabling Mn^{3+} regeneration through complexation [9,19,40]. While the exact contribution of each radical species was not quantified, the observed improvements in TOC and turbidity removal under catalytic conditions, together with mechanistic consistency reported in similar systems, strongly suggest that both •OH and $O_2\bullet^-$ were involved in PSNP degradation. Future work should include targeted scavenger assays and ESR analysis to confirm the dominant oxidative pathways.

Recent research has emphasized the importance of surface interactions in these systems. Liu et al. (2024) demonstrated that MnO_2–OA surface complexes (particularly β-MnO_2) improve ROS generation through electron transfer and oxygen vacancy formation [19]. Similarly, Wang et al. (2023) observed that MnO_2–oxalate interactions in δ-MnO_2 systems support continuous ROS cycling, optimizing pollutant degradation [42].

2.3. Effects of pH and Ozone Dosage

Although the combination of MnO_2 and OA exhibited a higher removal efficiency compared to other systems, the TOC removal achieved was just 10% under the tested experimental conditions. This underscores the necessity of optimizing operational parameters to enhance overall removal efficiency.

The efficiency of catalytic ozonation is strongly influenced by pH and O_3 dosage, as these parameters dictate the formation, stability, and reactivity of ROS. pH affects both ozone decomposition kinetics and the surface charge of the MnO_2 catalyst, while O_3 dosage determines oxidant availability and mass transfer efficiency [43,44].

To evaluate these effects, experiments were conducted at different initial pH values (3, 4, 7, 9, 11, and 12) and different O_3 doses ranging between 7.5 and 37.5 mg min^{-1}. The catalytic performance was assessed by monitoring TOC removal and turbidity reduction as indicators of PSNP degradation. Figure 3 shows the influence of pH on the degradation of PSNPs based on the TOC/TOC_0 ratios observed after 30 min of reaction using the MnO_2 + OA + O_3 system.

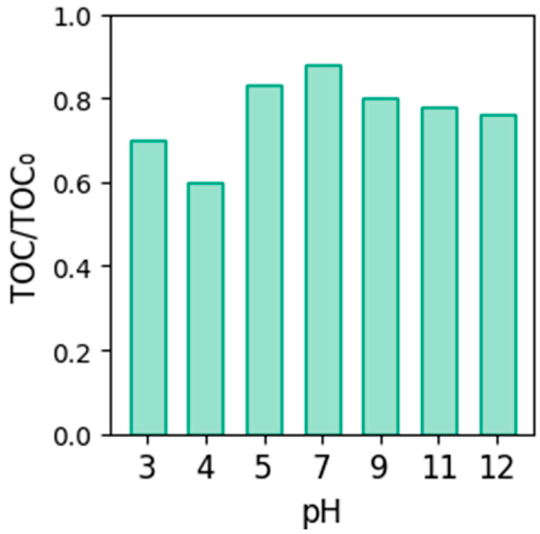

Figure 3. Effect of pH on TOC removal through catalytic ozonation ($[PSNP]_0$ = 20 mg L^{-1}, $[MnO_2]$ = 0.25 g L^{-1}, [OA] = 2.5 mg L^{-1}, O_3 dose= 7.5 mg min^{-1}, t = 30 min).

The results reveal that both pH and O_3 dosage play critical roles in the effectiveness of catalytic ozonation. At pH_0 = 4 and 7.5 mg min^{-1} of ozone dose, TOC removal reached 40% after 30 min, demonstrating the highest catalytic ozonation efficiency across all tested conditions (Figure 3). This improvement can be attributed to enhanced O_3 stability at acidic pH, reducing its self-decomposition into oxygen; strong adsorption of negatively charged ozone intermediates (O_3^-) and oxalate species ($C_2O_4^{2-}$) onto the positively charged MnO_2 surface; and the formation of Mn^{3+}–oxalate complexes, which facilitate redox cycling and sustained ROS generation [40]. These factors collectively improve the efficiency of catalytic ozonation by increasing ROS availability for PSNP oxidation. Similar effects were reported in previous studies, where carboxylate ligands, such as oxalate, stabilized Mn^{3+} and enhanced radical formation under acidic conditions [19]. Under near-neutral conditions

(pH ≈ pH_{PZC}), TOC removal was not as effective when compared to the results found under acidic conditions. At pH_0 = 7, TOC removal dropped significantly (TOC/TOC_0 = 0.88 at 7.5 mg min^{-1} ozone dose), indicating that near-neutral conditions were suboptimal for catalytic ozonation. This decrease in efficiency can be attributed to limited adsorption of O_3 and oxalate species, as the MnO_2 surface charge is close to neutral, and lower production of ROS [43]. These findings align with reports from Li et al. (2023), who observed a similar decline in catalytic ozonation performance for CeOx@MnOx catalysts at neutral pH [13]. At alkaline conditions, pH_0 between 9 and 12 ($pH_0 > pH_{PZC}$), TOC removal improved compared to neutral conditions (TOC/TOC_0 = 0.78 at pH_0 =11). This is consistent with the higher rate of O_3 self-decomposition into $^{\bullet}OH$ in alkaline media, indicating that radical-based oxidation plays a key role in alkaline conditions [40].

Figure 4 illustrates the effect of increasing ozone dose (7.5–37.5 mg min^{-1}) on the removal of TOC (Figure 4a) and turbidity (Figure 4b) through single ozonation and catalytic ozonation systems after 30 min of reaction. In terms of TOC removal, catalytic ozonation consistently outperformed single ozonation across all tested doses. At the highest dose of 37.5 mg min^{-1}, TOC/TOC_0 reached 0.48 for catalytic ozonation, compared to 0.65 for single ozonation. These results indicate that the catalytic system responds more effectively to increased ozone input, enhancing pollutant degradation through intensified ROS generation. Regarding turbidity removal, catalytic ozonation also demonstrated superior performance. The turbidity/$turbidity_0$ ratio decreased from 0.63 to 0.56 for catalytic ozonation across the tested ozone doses, while single ozonation only reached 0.84 at its lowest. This indicates not only greater chemical degradation but also enhanced disaggregation of PSNP aggregates through catalytic ozonation, supporting the role of ROS in disrupting particle cohesion [8].

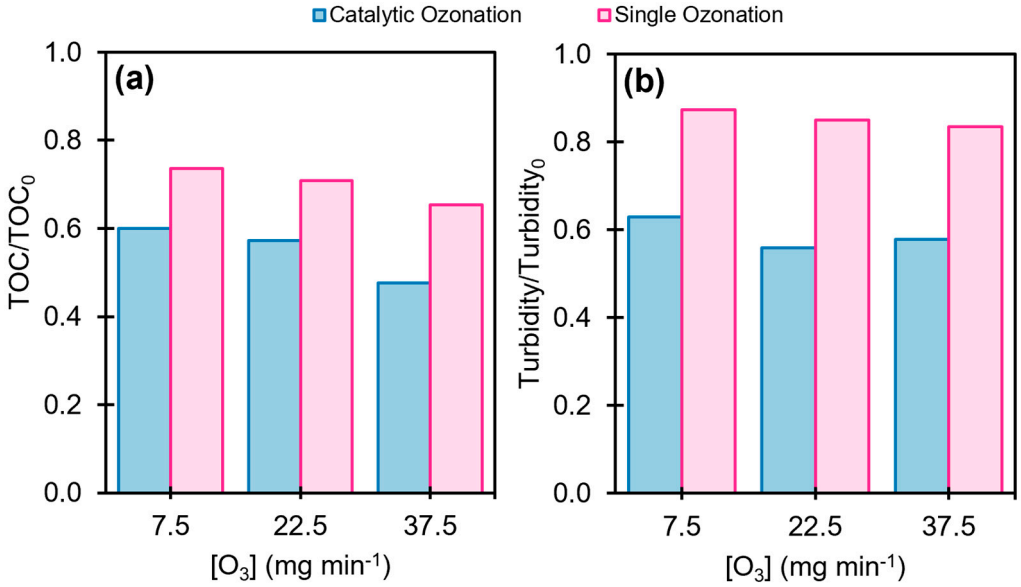

Figure 4. Effect of O_3 dose on TOC (**a**) and turbidity (**b**) removal through single ozonation and catalytic ozonation after 30 min ($[PSNP]_0$ = 20 mg L^{-1}, $[MnO_2]$ = 0.25 g L^{-1}, [OA] = 2.5 mg L^{-1}, pH_0 = 4).

2.4. Effect of Pyrolusite and Oxalic Acid Doses

The efficiency of catalytic ozonation can depend significantly on the concentration of both MnO_2 and OA, as these components work synergistically to promote the generation of ROS and maintain catalyst activity. Figure 5 provides insight into the synergistic interactions between MnO_2 and OA by identifying the optimal operating conditions for PSNP removal.

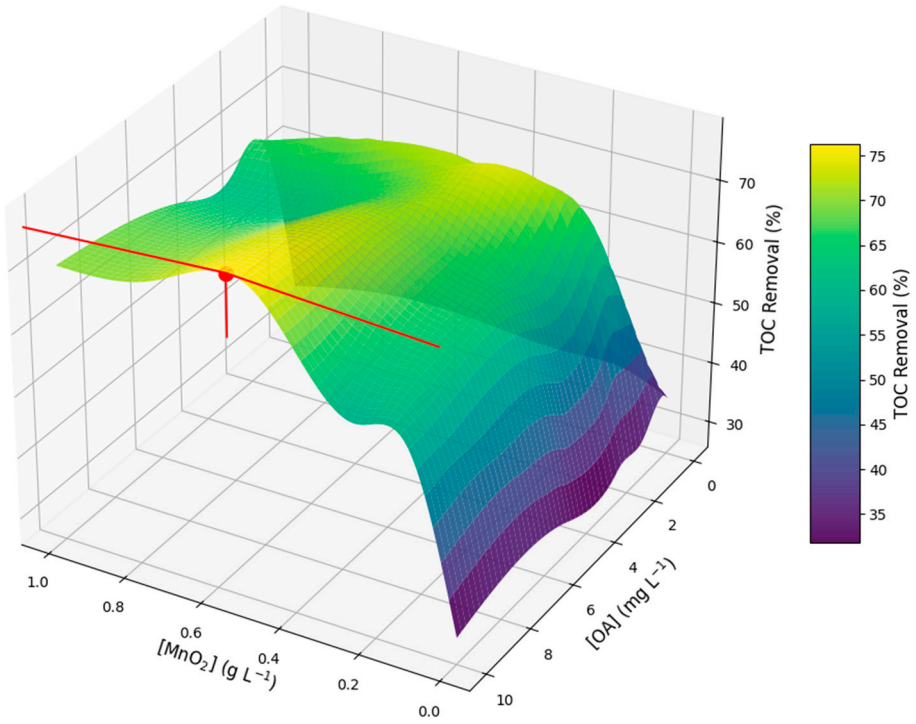

Figure 5. Surface response plot of the effects of MnO_2 and OA doses on TOC removal upon catalytic ozonation ($[PSNP]_0$ = 20 mg L^{-1}, O_3 dose= 37.5 mg min^{-1}, t = 30 min, pH_0 = 4). The red dot and line indicate the maximum TOC removal point identified in the response surface.

As shown in Figure 5, increasing MnO_2 concentration from 0 to 0.5 g L^{-1} led to a progressive enhancement in TOC removal, achieving a maximum efficiency of 75% at 0.5 g L^{-1} when combined with 10 mg L^{-1} of OA. This increased removal efficiency is attributed to the greater availability of active Mn sites, which facilitate O_3 decomposition into ROS, in agreement with previous observations regarding the role of transition metal oxides in catalytic ozonation. However, at concentrations exceeding 0.5 g L^{-1}, the efficiency plateaued and exhibited a slight decline, suggesting that an excessive MnO_2 load may promote ROS scavenging and contribute to catalyst agglomeration, limiting the availability of active sites. Similar trends have been reported for Mn-based ozonation catalysts, where excessive catalyst loading resulted in non-productive $^{\bullet}OH$ consumption and reduced pollutant degradation efficiency [11,34].

The presence of OA also played a crucial role in sustaining catalyst activity and maintaining continuous ROS generation, as indicated by the increase in TOC removal with OA concentration up to 10 mg L^{-1}. This effect is primarily due to the formation of Mn^{3+}–oxalate complexes, which prevent the accumulation of inactive Mn species and promote continuous redox cycling, ensuring the sustained production of ROS. However, when OA concentrations exceeded 10 mg L^{-1}, a reduction in PSNP degradation was observed, likely due to excessive radical scavenging, as organic acids can react with $^{\bullet}OH$, $O_2^{\bullet-}$, and O_3, reducing their availability for polymer oxidation. This observation is consistent with previous reports on the dual role of OA as both a radical promoter and a scavenger depending on its concentration [45,46].

A strong synergistic interaction between MnO_2 and OA was observed, as neither component alone achieved comparable TOC removal efficiencies. In the absence of OA, TOC removal remained below 40%, reinforcing the necessity of OA in preventing catalyst deactivation and enhancing ROS generation. This cooperative effect is further supported by previous studies [9,16,19] demonstrating that MnO_2–oxalate complexes enhance O_3

decomposition by stabilizing Mn^{3+} intermediates and increasing oxygen vacancy formation on the catalyst surface.

The highest PSNPs degradation efficiency was achieved at 0.5 g L^{-1} of MnO_2 and 10 mg L^{-1} of OA, reinforcing the importance of optimizing their ratio to maximize ROS formation while minimizing scavenging effects.

To assess the structural integrity of the PSNPs and confirm the occurrence of chemical degradation during ozonation, FTIR spectra were obtained for three samples: (i) the concentrated stock solution (50,000 mg L^{-1}), (ii) the diluted PSNP solution used in the experiments (20 mg L^{-1}), and (iii) the treated sample after 30 min of ozonation. Results are shown in Figure 6.

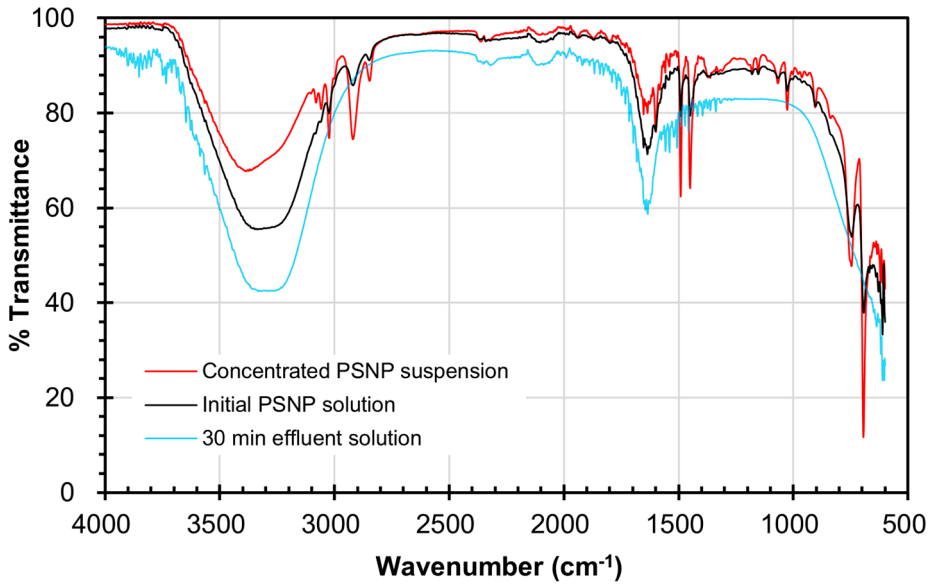

Figure 6. FTIR spectra of PSNPs: concentrated reference solution (red), initial solution of catalytic ozonation reaction (black), and effluent after 30 min reaction (blue) ($[PSNP]_0$ = 20 mg L^{-1}, O_3 dose = 37.5 mg min^{-1}, pH_0 = 4, $[MnO_2]$ = 0.5 g L^{-1}, [OA] = 10 mg L^{-1}).

In Figure 6, the initial spectrum of the PSNPs revealed characteristic absorption bands of polystyrene, including peaks at ~3025 cm^{-1} (C–H stretching of the aromatic ring), ~2920 and 2850 cm^{-1} (aliphatic C–H stretching), ~1600 cm^{-1} and ~1490 cm^{-1} (C=C stretching of the benzene ring), ~1452 cm^{-1} (CH_2 bending), and ~758 cm^{-1} and 698 cm^{-1} (out-of-plane bending of aromatic C–H) at both the concentrated PSNP suspension and the initial PSNP solution [47]. These assignments are consistent with the studies from di Luca et al. (2024) on PSNPs characterization [48]. After 30 min of ozonation, a notable decrease in intensity was observed for the bands associated with aromatic structures, particularly in the region from 1600 to 700 cm^{-1}, indicating that the ozonation process led to the cleavage of the benzene rings and progressive breakdown of the polymer chains. This behavior is consistent with the known reactivity of ozone, which initiates electrophilic attack on electron-rich aromatic rings, forming hydroxylated intermediates and ultimately yielding smaller oxygenated species and CO_2. The observed spectral changes, in combination with TOC and turbidity reductions, reinforce the evidence of PSNP degradation under the applied catalytic ozonation conditions.

Figure 7 illustrates the reduction in TOC over 120 min reaction time during the removal of PSNPs by catalytic ozonation (MnO_2 + OA + O_3) and single ozonation (O_3 only). The results clearly demonstrate the superior performance of catalytic ozonation, with TOC decreasing significantly faster and achieving a notable final reduction (~80%) compared to single ozonation (~37%). It must be noted that, during the early phase

of the reaction (0–30 min), the difference in performance between catalytic and single ozonation is most pronounced. By the 30 min mark, the TOC/TOC_0 ratio for catalytic ozonation had decreased to 0.2768, while single ozonation only reached 0.6528, indicating that the catalytic system achieves a removal rate that is more than twice as effective as ozone alone. As the reaction progresses, the TOC reduction rate slows down, which is common in ozonation processes due to the accumulation of oxidation by-products (e.g., carboxylic acids, aldehydes) that are more resistant to oxidation. This plateau effect is more noticeable in the single ozonation process, where the lack of continuous ROS production limits further degradation. In contrast, catalytic ozonation maintains higher efficiency due to the sustained generation of ROS on the MnO_2 surface, highlighting the benefits of the combined MnO_2 and OA catalytic system.

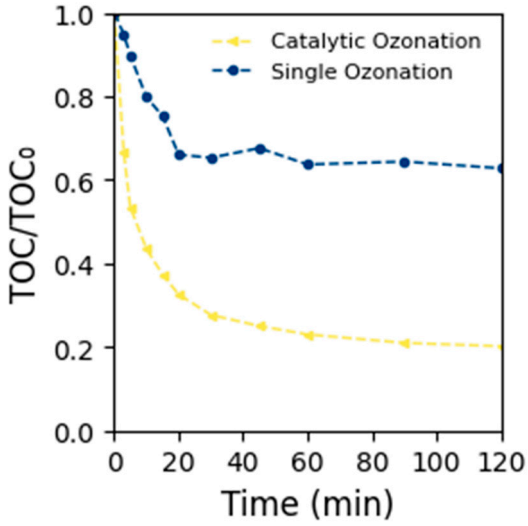

Figure 7. TOC reduction evolution upon catalytic ozonation and single ozonation of PSNPs ($[PSNP]_0$ = 20 mg L^{-1}, O_3 dose = 37.5 mg min^{-1}, pH_0 = 4, $[MnO_2]$ = 0.5 g L^{-1}, [OA] = 10 mg L^{-1}).

2.5. Catalyst Reusability

While catalytic ozonation demonstrated a faster and more substantial TOC decrease, its practical implementation also requires an understanding of catalyst durability. To address this, a study on catalyst reusability was conducted over three consecutive reuse cycles, and the results are shown in Figure 8. The catalyst (n-MnO_2) was dried at 80 °C overnight between cycles.

A progressive decline in removal efficiency was observed. In the first cycle, the system achieved a removal efficiency of 75%, which decreased to 73% in the second cycle and further to 66% in the third cycle. This gradual decrease in efficiency highlights the gradual deactivation of the MnO_2 catalyst, a phenomenon commonly observed in catalytic ozonation systems [19,49].

One of the primary causes of catalyst deactivation could be surface fouling by oxidation by-products. As PSNPs undergo oxidation, intermediate by-products, such as carboxylic acids and aldehydes, are generated. These intermediates can adsorb onto the surface of MnO_2, blocking active sites and reducing the availability of sites for O_3 decomposition. The accumulation of these by-products increases with each successive cycle, explaining the observed reduction in removal efficiency [43,50].

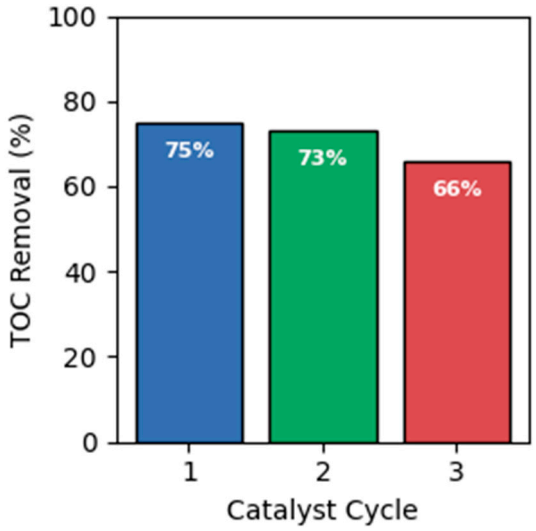

Figure 8. TOC removal efficiency of PSNPs after 30 min during three consecutive cycles ($[PSNP]_0$ = 20 mg L^{-1}, pH = 4, O_3 dose = 37.5 mg min^{-1}, t = 30 min, $[MnO_2]$ = 0.5 g L^{-1}, [OA] = 10 mg L^{-1}). Bar colors are used solely to differentiate catalyst cycles and do not represent additional variables.

Catalyst leaching is another factor that may contribute to the decline in performance. Under acidic conditions, manganese may dissolve into the solution, releasing Mn^{2+} ions into the reaction medium. This process reduces the active catalyst mass available for ROS production. Manganese leaching was measured during the study, and no leaching was detected, indicating that the MnO_2 catalyst remained stable throughout the reaction cycles. This result contrasts with findings from other studies on MnO_2-based catalytic ozonation systems, where leaching has been identified as a potential deactivation mechanism [51,52].

Despite these deactivation mechanisms, it is important to note that the efficiency decreased by only 12% after three consecutive cycles, indicating that the MnO_2-based system maintains a notable activity. This result suggests that, although some loss of catalytic activity occurs, the system remains viable for extended use. To improve catalyst durability, several regeneration strategies could be considered, such as thermal reactivation, oxidative washing, or chemical cleaning to remove fouling agents [50,53].

3. Materials and Methods

3.1. Materials and Reagents

The materials used in this study included PSNPs, catalysts, co-catalysts, ozone gas, and various reagents essential for experimental procedures and analytical measurements. The PSNPs were commercially available (microParticles GmbH, Berlin, Germany) and characterized by a nominal mean diameter of 140 nm. Detailed physicochemical characterization of this commercial PSNPs suspension was previously reported in recent studies [39,48,54], including transmission electron microscopy (TEM), dynamic light scattering (DLS), and nanoparticle tracking analysis (NTA). These analyses confirmed the nanoscale size and spherical morphology of the particles, with a DLS hydrodynamic diameter of 149.7 nm (PDI = 0.06), modal size of 135.9 nm (NTA), and mean diameter of 137.4 nm observed by TEM. Optical and chemical characteristics were also confirmed by UV–Vis spectroscopy (λ = 223 nm) and FTIR (700–760 cm^{-1}), consistent with polystyrene signatures. These particles were used without further modification. The commercial PSNPs solution was 50,000 mg L^{-1}. Natural MnO_2 in its pyrolusite form was used as the primary catalyst due to its availability, low cost, and high redox potential. This naturally occurring mineral was used as a heterogeneous catalyst without prior modification or pretreatment, with a

particle size distribution ranging from 25 µm to 70 µm. The natural manganese dioxide (MnO_2) used in this study was obtained from Suministros Anper S.L. (Barcelona, Spain), under the reference OX841027. The chemical composition of the natural pyrolusite (MnO_2) used in this study, as reported by the supplier, is as follows: 78.4% MnO_2, 5.39% Al_2O_3, 3.76% SiO_2, 3.78% Fe_2O_3, and 0.2% P_2O_5. The material was used without further purification. An additional ICP-MS analysis (Thermo Scientific iCAP RQ, Waltham, MA, USA) confirmed Mn as the predominant element (~73.5 wt.%), with minor Fe content (~3.2 wt.%), consistent with the supplier's data. The co-catalyst used in this study was analytical-grade oxalic acid (purity $\geq$ 99%), which was sourced from Panreac, AppliChem, Barcelona, Spain. Hydrochloric acid (HCl, 37%) and sodium hydroxide (NaOH, $\geq$97%) were both obtained from Sigma-Aldrich (Merck KGaA, Darmstadt, Germany) and used for pH adjustments throughout the experimental procedures.

3.2. Experimental Setup and Procedure

The experimental setup consisted of a semi-batch reactor equipped with a continuous O_3 inlet. The borosilicate glass vessel reactor had a volume of 1.5 L and was continuously stirred at 800 rpm to ensure homogeneity of the reaction medium. The temperature was maintained at 25 $\pm$ 2 °C (room temperature) throughout all experiments.

Ozone (O_3) gas was generated in situ using an ozone generator (Model 301.19, Sander Elektrogerätebau GmbH, Uetze, Germany) and was introduced at a constant flow rate of 0.75 L min^{-1} and a concentration of 10 mg L^{-1}, unless otherwise indicated, through a porous diffuser located at the base of the reactor. A gas trap containing an aqueous potassium iodide (KI) solution was used to capture unreacted O_3, preventing its release into the laboratory environment.

The PSNPs suspension was prepared by diluting the commercial solution of PSNPs to a target concentration of 20 mg L^{-1} in ultrapure deionized water (resistivity $\geq$ 18.2 MΩ·cm). The pH of the solution was adjusted to the desired initial pH (3–11) using 0.1 M HCl or 0.1 M NaOH. Then, MnO_2 and OA were introduced in this order. The initial concentration of both was investigated in the range from 0.125 to 1 g L^{-1} and from 1.25 to 10 mg L^{-1}, respectively. Moreover, O_3 dose was evaluated between 7.5 and 37.5 mg min^{-1}.

Control experiments were conducted to assess the effects of single ozonation (without MnO_2 or OA) and to evaluate the performance of catalytic ozonation under different conditions. Blank tests (without PSNPs) were also performed to check for background interference. All experiments were performed in triplicate, and the experimental data reported represent the average values of these replicates to ensure consistency and reproducibility.

3.3. Analytical Methods

Samples were periodically withdrawn from the reactor and filtered when necessary to separate catalyst particles and analyzed using fiberglass membranes with an average pore diameter below 1 µm (Sartorius Glass Microfiber Filters, 13400-47-Q, Sartorius AG, Göttingen, Germany).

Turbidity was measured using a turbidimeter (Model 2100P, Hach Company, Düsseldorf, Germany), following the ISO 7027 method [55]. Turbidity was recorded at regular intervals during each experiment to monitor the physical disaggregation of PSNPs. Changes in turbidity provided indirect evidence of PSNP breakdown [39].

TOC analysis was performed using a TOC analyzer (multi N/C 3100 Series, Analytik Jena GmbH, Jena, Germany), which quantifies the total concentration of organic carbon in the aqueous phase. TOC reflects the chemical degradation of PSNPs, as it captures the conversion of polymeric carbon into dissolved intermediates or complete mineralization

into CO_2. TOC samples were filtered to remove catalyst particles before analysis. All measurements were conducted in triplicate, and the results were reported as mean values.

Manganese leaching was assessed to evaluate the stability of the MnO_2 catalyst during the ozonation process. The elemental composition of the MnO_2 catalyst was evaluated using inductively coupled plasma mass spectrometry (ICP-MS, iCAP RQ, Thermo Scientific Inc., Waltham, MA, USA), providing semiquantitative data on Mn and Fe content in the solid material. This analysis confirmed that manganese release was not significant under the tested conditions, ensuring the stability and reusability of the catalyst.

Fourier-transform infrared (FTIR) spectra were acquired using a spectrometer (Cary 630 FTIR, Agilent Technologies Inc., Santa Clara, CA, USA) equipped with a single-reflection diamond ATR (attenuated total reflectance) accessory, to evaluate the chemical structure of PSNPs before and after ozonation. The measurements were carried out in the spectral range of 4000–500 cm^{-1}, with a resolution of 4 cm^{-1} and 32 scans per sample. The ATR crystal is composed of type IIa diamond, providing high chemical resistance and an optimal IR signal for polymeric materials. Prior to each analysis, the sample press was used to ensure proper contact between the PSNP powders and the crystal surface.

3.4. Catalyst Characterization

The characterization of the n-MnO_2 catalyst was conducted using three complementary techniques: Fourier-transform infrared spectroscopy (FTIR), pH at the point of zero charge (pH_{PZC}) determination, and X-ray photoelectron spectroscopy (XPS). These techniques provided insights into the surface functional groups, chemical bonding, and oxidation states of manganese species, which are critical for understanding the catalytic behavior of pyrolusite during the ozonation of PSNPs.

The FTIR spectra of the catalyst were obtained using a PerkinElmer Spectrum Two™ FTIR spectrometer (PerkinElmer Inc., Shelton, CT, USA). The analyses were performed by recording multiple scans across a wavenumber range of 450 to 4000 cm^{-1} to identify the vibrational modes of surface functional groups. This spectral range encompasses characteristic peaks associated with manganese–oxygen bonding, as well as the presence of hydroxyl groups that can influence catalytic ozonation performance.

The FTIR technique was employed to elucidate the chemical interactions occurring on the surface of pyrolusite, particularly the role of hydroxyl groups in the adsorption and decomposition of O_3. The data collected were subsequently analyzed to correlate the structural characteristics of the catalyst with its catalytic efficiency in PSNP degradation.

The elemental composition and oxidation states of manganese within the pyrolusite catalyst were investigated using a PHI VersaProbe 4 Scanning XPS Microprobe (ULVAC-PHI Inc., Chanhassen, MN, USA). This surface-sensitive technique enabled the identification of manganese species and their respective oxidation states, which are directly related to the catalytic activity of the material.

The XPS measurements were performed by irradiating the sample with a monochromatic Al Kα X-ray source (1486.6 eV) and recording the photoelectron emission from the Mn2p and O1s regions. The high-resolution spectra were deconvoluted to distinguish between different manganese oxidation states, particularly Mn^{3+} and Mn^{4+}, which play a key role in the generation of ROS during ozonation.

Additionally, the pH_{PZC} of the pyrolusite catalyst was determined using the batch equilibrium method. This analysis provides insights into the surface charge properties of the material, which influence its interaction with O_3 and organic pollutants. The pH_{PZC} was obtained by suspending the catalyst in deionized water at different initial pH values (adjusted using 0.1 M HCl or 0.1 M NaOH), followed by equilibration for 24 h. The final pH was then measured, and the pH_{PZC} was identified as the pH at which no net surface

charge was observed on the catalyst surface. This parameter is essential for understanding the adsorption behavior of reactive species during the catalytic ozonation process.

4. Conclusions

The growing presence of PSNPs in aquatic environments poses significant environmental and health risks due to their chemical stability, small size, and bioavailability. This study demonstrates the potential of catalytic ozonation as an effective method for PSNP removal, particularly when enhanced by the synergistic action of natural pyrolusite (n-MnO_2) and OA. Operational parameters were evaluated, including pH, applied O_3 dose, OA, and catalyst concentration, providing a comprehensive understanding of the effects of each operational parameter on PSNP degradation.

The results reveal that the combination of MnO_2 and OA significantly enhances the generation of ROS compared to single ozonation or the use of MnO_2 alone. The optimal conditions for PSNP removal were observed at pH 4, with an O_3 dose of 37.5 mg min^{-1}, 0.5 g L^{-1} of MnO_2, and 10 mg L^{-1} of OA. Under these conditions, the system achieved a maximum TOC removal of 75% after 30 min ozonation, with a notable improvement in turbidity reduction, reflecting both the chemical degradation and physical disaggregation of PSNP aggregates. These findings underscore the importance of catalyst–co-catalyst interactions in promoting ROS generation and enhancing oxidation efficiency.

Beyond removal efficiency, the reusability of the MnO_2 catalyst was evaluated across consecutive reaction cycles. Although a slight decline in removal efficiency was observed (from 74.69% to 65.73% after three cycles), the catalyst retained most of its activity without detecting manganese leaching, indicating its potential for repeated use in water treatment systems. This durability positions MnO_2 as a promising candidate for scalable applications, especially when paired with low-cost natural pyrolusite, a readily available source of MnO_2.

Author Contributions: Conceptualization, V.M. and J.N.-S.; methodology, V.M. and J.N.-S.; validation, V.M., J.N.-S. and C.S.; formal analysis, V.M.; investigation, V.M. and J.N.-S.; resources, M.D. and C.S.; data curation, V.M.; writing—original draft preparation, V.M.; writing—review and editing, J.N.-S., M.D. and C.S.; visualization, V.M. and J.N.-S.; supervision, M.D. and C.S.; project administration, C.S.; funding acquisition, M.D. and C.S. All authors have read and agreed to the published version of the manuscript.

Funding: This work was financially supported through the projects TED2021-131569B-I00 by MCIN/AEI/10.13039/501100011033, Next Generation EU/PRTR; PID2023-146338OB-I00 by MCIU/AEI/10.13039/501100011033/ FEDER,UE; as well as by the Coordenação de Aperfeiçoamento de Pessoal de Nível Superior—Brasil (CAPES), Finance Code 001. Additional financial support was provided by Fundação Carlos Chagas Filho de Amparo à Pesquisa do Estado do Rio de Janeiro (FAPERJ), under projects E-26/204.177/2024 and E-26/200.979/2021, and by the Conselho Nacional de Desenvolvimento Científico e Tecnológico (CNPq), project 304175/2020-0.

Data Availability Statement: The original contributions presented in this study are included in the article. Further inquiries can be directed to the corresponding authors.

Acknowledgments: The authors thank the Surface Analysis Laboratory of the CCiTUB for carrying out the XPS measurements. Victor Mello thanks CAPES for the PRINT scholarship through the research projects 88887.311613/2018-00 (UFRJ) and 88887.310122/2018-00 (UFRJ).

Conflicts of Interest: The authors declare no conflicts of interest. The funders had no role in the design of the study; in the collection, analyses, or interpretation of data; in the writing of the manuscript; or in the decision to publish the results.

Abbreviations

The following abbreviations are used in this manuscript:

AOP	Advanced oxidation process
FTIR	Fourier-transform infrared spectroscopy
GPC	Gel permeation chromatography
MnO_2	Manganese dioxide
MP	Microplastic
NP	Nanoplastic
n-MnO_2	Natural manganese dioxide (pyrolusite)
OA	Oxalic acid
O_3	Ozone
$^{\bullet}OH$	Hydroxyl radical
$O_2^{\bullet-}$	Superoxide radical
pH_{PZC}	Point of zero charge
PS	Polystyrene
PSNPs	Polystyrene nanoplastics
ROS	Reactive oxygen species
TOC	Total organic carbon
XPS	X-ray photoelectron spectroscopy

References

1. Koelmans, A.A.; Besseling, E.; Foekema, E.; Kooi, M.; Mintenig, S.; Ossendorp, B.C.; Redondo-Hasselerharm, P.E.; Verschoor, A.; Van Wezel, A.P.; Scheffer, M. Risks of Plastic Debris: Unravelling Fact, Opinion, Perception, and Belief. *Environ. Sci. Technol.* **2017**, *51*, 11513–11519. [CrossRef] [PubMed]
2. Wright, S.L.; Kelly, F.J. Plastic and Human Health: A Micro Issue? *Environ. Sci. Technol.* **2017**, *51*, 6634–6647. [CrossRef] [PubMed]
3. Gigault, J.; ter Halle, A.; Baudrimont, M.; Pascal, P.Y.; Gauffre, F.; Phi, T.L.; El Hadri, H.; Grassl, B.; Reynaud, S. Current Opinion: What Is a Nanoplastic? *Environ. Pollut.* **2018**, *235*, 1030–1034. [CrossRef] [PubMed]
4. European Commission Directive (EU). 2020/2184 on the Quality of Water Intended for Human Consumption. *Off. J. Eur. Union* **2020**, *L435*, 1–62.
5. Andrady, A.L. Microplastics in the Marine Environment. *Mar. Pollut. Bull.* **2011**, *62*, 1596–1605. [CrossRef]
6. Song, Y.K.; Hong, S.H.; Jang, M.; Kang, J.H.; Kwon, O.Y.; Han, G.M.; Shim, W.J. Large Accumulation of Micro-Sized Synthetic Polymer Particles in the Sea Surface Microlayer. *Environ. Sci. Technol.* **2014**, *48*, 9014–9021. [CrossRef]
7. Wagner, M.; Lambert, S. Freshwater Microplastics: Emerging Environmental Contaminants? In *The Handbook of Environmental Chemistry*; Barceló, D., Kostianoy, A.G., Eds.; Springer International Publishing: Cham, Switzerland, 2018; Volume 58, ISBN 978-3-319-61614-8. [CrossRef]
8. von Gunten, U. Ozonation of Drinking Water: Part I. Oxidation Kinetics and Product Formation. *Water Res.* **2003**, *37*, 1443–1467. [CrossRef]
9. Xiao, H.; Liu, R.; Zhao, X.; Qu, J. Enhanced Degradation of 2,4-Dinitrotoluene by Ozonation in the Presence of Manganese(II) and Oxalic Acid. *J. Mol. Catal. A Chem.* **2008**, *286*, 149–155. [CrossRef]
10. Issaka, E.; AMU-Darko, J.N.O.; Yakubu, S.; Fapohunda, F.O.; Ali, N.; Bilal, M. Advanced Catalytic Ozonation for Degradation of Pharmaceutical Pollutants—A Review. *Chemosphere* **2022**, *289*, 133208. [CrossRef]
11. Rekhate, C.V.; Srivastava, J.K. Recent Advances in Ozone-Based Advanced Oxidation Processes for Treatment of Wastewater—A Review. *Chem. Eng. J. Adv.* **2020**, *3*, 100031. [CrossRef]
12. Issaka, E.; Baffoe, J.; Adams, M. Exploring Heterogeneous Catalytic Ozonation: Catalyst Types, Reaction Mechanisms, Applications, Challenges, and Future Outlook. *Sustain. Chem. Environ.* **2024**, *8*, 100185. [CrossRef]
13. Li, Y.; Zhang, C.; Shen, C.; Jiang, G.; Guan, B. Enhanced Ozonation of Polystyrene Nanoplastics in Water with CeOx@MnOx Catalyst. *Environ. Res.* **2023**, *220*, 115220. [CrossRef] [PubMed]
14. Isibor, P.O.; Devi, G.; Enuneku, A.A. (Eds.) *Environmental Nanotoxicology Combatting the Minute Contaminants*; Springer: Berlin/Heidelberg, Germany, 2024; ISBN 978-3-031-54153-7.
15. Huang, J.; Dai, Y.; Singewald, K.; Liu, C.C.; Saxena, S.; Zhang, H. Effects of MnO_2 of Different Structures on Activation of Peroxymonosulfate for Bisphenol A Degradation under Acidic Conditions. *Chem. Eng. J.* **2019**, *370*, 906–915. [CrossRef]
16. Andreozzi, R.; Insola, A.; Caprio, V.; D'Amore, M.G. The Kinetics of Mn(II)-Catalysed Ozonation of Oxalic Acid in Aqueous Solution. *Water Res.* **1992**, *26*, 917–921. [CrossRef]

17. Andreozzi, R.; Caprio, V.; Giovanna D'amore, M.; Insola, A. Manganese Catalysis in Water Pollutants Abatement by Ozone. *Environ. Technol.* **1995**, *16*, 885–891. [CrossRef]
18. Nawrocki, J.; Kasprzyk-Hordern, B. The Efficiency and Mechanisms of Catalytic Ozonation. *Appl. Catal. B Environ.* **2010**, *99*, 27–42. [CrossRef]
19. Liu, J.; Yuan, X.; Sans, C. Insights into the Role of β-MnO_2 and Oxalic Acid Complex Expediting Ozonation: Structural Properties and Mechanism. *Sep. Purif. Technol.* **2024**, *341*, 126904. [CrossRef]
20. Omorogie, M.O.; Agbadaola, M.T.; Olatunde, A.M.; Helmreich, B.; Babalola, J.O. Surface Equilibrium and Dynamics for the Adsorption of Anionic Dyes onto MnO2/Biomass Micro-Composite. *Green Chem. Lett. Rev.* **2022**, *15*, 49–58. [CrossRef]
21. Dubal, D.P.; Kim, W.B.; Lokhande, C.D. Galvanostatically Deposited Fe: MnO2 Electrodes for Supercapacitor Application. *J. Phys. Chem. Solids* **2012**, *73*, 18–24. [CrossRef]
22. Yu, Y.; Li, X.; Zhang, R.; Guo, W. Insights into the Morphology-Dependent Adsorption of Aged Polystyrene Nanoplastics on Manganese Oxides. *Colloids Surfaces A Physicochem. Eng. Asp.* **2023**, *679*, 132565. [CrossRef]
23. Pang, M.; Long, G.; Jiang, S.; Ji, Y.; Han, W.; Wang, B.; Liu, X.; Xi, Y. Rapid Synthesis of Graphene/Amorphous α-MnO2 Composite with Enhanced Electrochemical Performance for Electrochemical Capacitor. *Mater. Sci. Eng. B* **2015**, *194*, 41–47. [CrossRef]
24. Kumar, Y.; Chopra, S.; Gupta, A.; Kumar, Y.; Uke, S.J.; Mardikar, S.P. Low Temperature Synthesis of MnO_2 Nanostructures for Supercapacitor Application. *Mater. Sci. Energy Technol.* **2020**, *3*, 566–574. [CrossRef]
25. Malvestiti, J.A.; Cavalcante, R.P.; Tornisielo, V.L.; Dantas, R.F. Metals as Catalysts for Ozonation. In *Heavy Metals–Recent Advances*; Almayyahi, B., Ed.; IntechOpen: London, UK, 2023; ISBN 978-1-83768-515-8.
26. Chen, S.; Shu, X.; Wang, H.; Zhang, J. Thermally Driven Phase Transition of Manganese Oxide on Carbon Cloth for Enhancing the Performance of Flexible All-Solid-State Zinc-Air Batteries. *J. Mater. Chem. A* **2019**, *7*, 19719–19727. [CrossRef]
27. Jiang, Y.; Ba, D.; Li, Y.; Liu, J. Noninterference Revealing of "Layered to Layered" Zinc Storage Mechanism of δ-MnO_2 toward Neutral Zn–Mn Batteries with Superior Performance. *Adv. Sci.* **2020**, *7*, 1902795. [CrossRef]
28. De la Cruz, I.J.; Rodríguez, S.J.L.; Fuentes, I.; Tiznado, H.; Vazquez-Arce, J.L.; Romero-Ibarra, I.; Guzmán, C.J.I.; Gutiérrez, H.M. Effect of Crystalline Phase of MnO2 on the Degradation of Bisphenol A by Catalytic Ozonation. *J. Environ. Chem. Eng.* **2023**, *11*, 110753. [CrossRef]
29. Zhang, W.; Hao, M.; Wang, Y.; Sun, P.; Zeng, D.; Wang, X.; Liang, P. Effect of PH on Microstructure and Catalytic Oxidation of Formaldehyde in MnO2 Catalyst. *Catalysts* **2023**, *13*, 490. [CrossRef]
30. Zhu, G.; Zhu, J.; Jiang, W.; Zhang, Z.; Wang, J.; Zhu, Y.; Zhang, Q. Surface Oxygen Vacancy Induced A-MnO2nanofiber for Highly Efficient Ozone Elimination. *Appl. Catal. B Environ.* **2017**, *209*, 729–737. [CrossRef]
31. Wang, Y.; Chen, L.; Cao, H.; Chi, Z.; Chen, C.; Duan, X.; Xie, Y.; Qi, F.; Song, W.; Liu, J.; et al. Role of Oxygen Vacancies and Mn Sites in Hierarchical Mn2O3/LaMnO3-Δ Perovskite Composites for Aqueous Organic Pollutants Decontamination. *Appl. Catal. B Environ.* **2019**, *245*, 546–554. [CrossRef]
32. Xia, L.; Liang, W.; Chen, G.; Li, W.; Gao, M. Catalytic Ozonation of Quinoline Utilizing Manganese-Based Catalyst with Abundant Oxygen Vacancies. *Catal. Letters* **2022**, *152*, 1669–1677. [CrossRef]
33. Radinger, H.; Connor, P.; Stark, R.; Jaegermann, W.; Kaiser, B. Manganese Oxide as an Inorganic Catalyst for the Oxygen Evolution Reaction Studied by X-Ray Photoelectron and Operando Raman Spectroscopy. *ChemCatChem* **2021**, *13*, 1175–1185. [CrossRef]
34. Luo, K.; Zhao, S.X.; Wang, Y.F.; Zhao, S.J.; Zhang, X.H. Synthesis of Petal-like δ-MnO_2 and Its Catalytic Ozonation Performance. *New J. Chem.* **2018**, *42*, 6770–6777. [CrossRef]
35. He, Y.; Wang, L.; Chen, Z.; Shen, B.; Wei, J.; Zeng, P.; Wen, X. Catalytic Ozonation for Metoprolol and Ibuprofen Removal over Different MnO2 Nanocrystals: Efficiency, Transformation and Mechanism. *Sci. Total Environ.* **2021**, *785*, 147328. [CrossRef]
36. Tang, W.; Wu, X.; Li, D.; Wang, Z.; Liu, G.; Liu, H.; Chen, Y. Oxalate Route for Promoting Activity of Manganese Oxide Catalysts in Total VOCs' Oxidation: Effect of Calcination Temperature and Preparation Method. *J. Mater. Chem. A* **2014**, *2*, 2544–2554. [CrossRef]
37. Kasprzyk-Hordern, B.; Ziółek, M.; Nawrocki, J. Catalytic Ozonation and Methods of Enhancing Molecular Ozone Reactions in Water Treatment. *Appl. Catal. B Environ.* **2003**, *46*, 639–669. [CrossRef]
38. Li, Y.; Li, J.; Ding, J.; Song, Z.; Yang, B.; Zhang, C.; Guan, B. Degradation of Nano-Sized Polystyrene Plastics by Ozonation or Chlorination in Drinking Water Disinfection Processes. *Chem. Eng. J.* **2022**, *427*, 131690. [CrossRef]
39. Nieto-Sandoval, J.; Ammar, R.; Sans, C. Enhancing Nanoplastics Removal by Metal Ion-Catalyzed Ozonation. *Chem. Eng. J. Adv.* **2024**, *19*, 100621. [CrossRef]
40. Rodríguez, A.; Rosal, R.; Perdigón-Melón, J.A.; Mezcua, M.; Agüera, A.; Hernando, M.D.; Letón, P.; Fernández-Alba, A.R.; García-Calvo, E. Ozone-Based Technologies in Water and Wastewater Treatment. *Handb. Environ. Chem. Vol. 5 Water Pollut.* **2008**, *5* (Suppl. S2), 127–175. [CrossRef]
41. Andreozzi, R.; Caprio, V.; Insola, A.; Marotta, R.; Tufano, V. The Ozonation of Pyruvic Acid in Aqueous Solutions Catalyzed by Suspended and Dissolved Manganese. *Water Res.* **1998**, *32*, 1492–1496. [CrossRef]

42. Wang, J.; Yue, W.; Teng, Y.; Zhai, Y.; Zhu, H. Degradation Kinetics and Transformation Pathway of Methyl Parathion by δ-MnO_2/Oxalic Acid Reaction System. *Chemosphere* **2023**, *320*, 138054. [CrossRef]
43. Psaltou, S.; Mitrakas, M.; Zouboulis, A. Heterogeneous Catalytic Ozonation: Solution PH and Initial Concentration of Pollutants as Two Important Factors for the Removal of Micropollutants from Water. *Separations* **2022**, *9*, 413. [CrossRef]
44. Fallah, N.; Bloise, E.; Santoro, D.; Mele, G. State of Art and Perspectives in Catalytic Ozonation for Removal of Organic Pollutants in Water: Influence of Process and Operational Parameters. *Catalysts* **2023**, *13*, 324. [CrossRef]
45. Wu, Z.; Abramova, A.; Nikonov, R.; Cravotto, G. Sonozonation (Sonication/Ozonation) for the Degradation of Organic Contaminants—A Review. *Ultrason. Sonochem.* **2020**, *68*, 105195. [CrossRef]
46. Zhao, Y.; An, H.; Dong, G.; Feng, J.; Ren, Y.; Wei, T. Elevated Removal of Di-n-Butyl Phthalate by Catalytic Ozonation over Magnetic Mn-Doped Ferrospinel ZnFe2O4 Materials: Efficiency and Mechanism. *Appl. Surf. Sci.* **2020**, *505*, 144476. [CrossRef]
47. Smith, B.C. The Infrared Spectra of Polymers V: Epoxies. *Spectroscopy* **2022**, *37*, 17–19. [CrossRef]
48. di Luca, C.; Garcia, J.; Munoz, M.; Hernando-Pérez, M.; de Pedro, Z.M.; Casas, J.A. Strategies for the Quantification and Characterization of Nanoplastics in AOPs Research. *Chem. Eng. J.* **2024**, *493*, 152490. [CrossRef]
49. Li, X.; Fu, L.; Chen, F.; Zhao, S.; Zhu, J.; Yin, C. Application of Heterogeneous Catalytic Ozonation in Wastewater Treatment: An Overview. *Catalysts* **2023**, *13*, 342. [CrossRef]
50. Cao, H.; Xie, Y.; Wang, Y.; Xiao, J. (Eds.) *Advanced Ozonation Processes for Water and Wastewater Treatment: Active Catalysts and Combined Technologies*; Royal Society of Chemistry: Cambridge, UK, 2022; ISBN 978-1-83916-389-0.
51. Nawaz, F.; Xie, Y.; Cao, H.; Xiao, J.; Wang, Y.; Zhang, X.; Li, M.; Duan, F. Catalytic Ozonation of 4-Nitrophenol over an Mesoporous α-MnO2 with Resistance to Leaching. *Catal. Today* **2015**, *258*, 595–601. [CrossRef]
52. Yang, K.; Yu, J.; Guo, Q.; Wang, C.; Yang, M.; Zhang, Y.; Xia, P.; Zhang, D.; Yu, Z. Comparison of Micropollutants' Removal Performance between Pre-Ozonation and Post-Ozonation Using a Pilot Study. *Water Res.* **2017**, *111*, 147–153. [CrossRef]
53. Saputra, E.; Muhammad, S.; Sun, H.; Ang, H.M.; Tadé, M.O.; Wang, S. Manganese Oxides at Different Oxidation States for Heterogeneous Activation of Peroxymonosulfate for Phenol Degradation in Aqueous Solutions. *Appl. Catal. B Environ.* **2013**, *142–143*, 729–735. [CrossRef]
54. Ortiz, D.; Munoz, M.; Nieto-Sandoval, J.; Romera-Castillo, C.; de Pedro, Z.M.; Casas, J.A. Insights into the Degradation of Microplastics by Fenton Oxidation: From Surface Modification to Mineralization. *Chemosphere* **2022**, *309*, 136809. [CrossRef]
55. ISO. *ISO 7027:2016*; Water Quality—Determination of Turbidity. International Organization for Standardization: Geneva, Switzerland, 2016.